Celal Bayar University Journal of Science

A Study on the Deformation Behavior of AA7075 Powder with Three-Dimensional Ball Mill

Gürkan Soy[1]*, Salih Korucu[2]

[1] Machine and Metal Technologies, Manisa Celal Bayar University, Manisa, Türkiye
[2] Department of Manufacturing Engineering, Gazi University, Ankara, Türkiye
*gurkan.soy@cbu.edu.tr
*Orcid: 0000-0002-0308-1702

Received: 27 January 2022
Accepted: 1 December 2022
DOI: 10.18466/cbayarfbe.1063777

Abstract

Aluminium-based composite materials are frequently preferred in many new-generation engineering applications due to their high strength, wear and corrosion resistance, improvement of mechanical properties, machinability, and low density. Mechanical alloying is essential in producing composites with high properties in powder metallurgy, which is one of the composite material production methods. In this study, the deformation of AA7075 powder was investigated with a three-dimensional ball mill designed and produced for use in mechanical alloying processes. In the milling processes, three different rotational speeds (150, 200 and 250 rpm), three different ball to powder ratios (5:1, 10:1 and 20:1) and three different milling times (30, 60 and 90 min) were used. The particle deformation was evaluated by particle size analysis and powder structure examination. The obtained results were analysed with analysis of variance, regression method, three-dimensional graphics, optical microscope and scanning electron microscope (SEM) images. When the results were examined, the maximum deformation and powder size among the selected experimental parameters were obtained at 150 rpm rotational speed, 20:1 ball to powder ratio, and 90 min.

Keywords: Powder Metallurgy, AA7075, Three-Dimensional Ball Mill.

1. Introduction

Metal Matrix Composites (MMC) [1–5] is an important material group that can be used to meet some essential needs of the modern industry thanks to its many properties, especially low density, high strength, increased wear resistance, and high operating temperature [6, 7]. Powder metallurgy (PM) method, which is frequently used in the production of MMCs, provides many advantages such as low material consumption and high production speed, production of sensitive and complex profile parts of alloys that are impossible or difficult to produce with other production methods [8]. Aluminium Matrix Composites (AMC), which can achieve better mechanical properties compared to traditional monolithic materials, have significant potential for industrial applications in the field of aerospace, automotive, electronics and machinery in the field of MMK due to their attractive properties [9].

Aluminium alloys are widely used in machinery, electronics, automotive and aerospace industries due to their high mechanical properties and high machinability as well as high electrical conductivity, high corrosion resistance, low density and fatigue resistance [10]. AA7075 is an important and indispensable material in the aviation industry and has reliable properties, especially for aircraft wing pylons, airframes and rocket production. However, despite its wide range of applications, aluminium alloy industrial applications need even higher strength to meet their specific requirements [11].

Mechanical alloying (MA), ductile-ductile, ductile-brittle, and brittle-brittle powder mixtures, which are applied to produce new alloys, are ground for the desired time until a similar structure is reached depending on the desired composition ratio of the composition of each powder particle. In the mechanical alloying process, metallic powders first take a flat shape in ductile materials and become cold-welded to each other as the deformation continues. With the milling time increase, the embrittlement powders are broken and the alloying process reaches a stable state after a specific cold welding-fracture cycle [12]. Essential

variables of the MA process are material, milling system, milling time, milling cycle, and ball to powder ratio [13, 14]. Different grinders such as SPEX [15–17], Planetary [18–22], and attritor [23–25] are generally used to produce mechanically alloyed powders. Although they have cooling, heating, etc., add-ons to increase the milling efficiency, they differ in their structures [13]. The standard devices used for the MA process generally grind in two dimensions and because the powders are affected by gravity, they are collected at the bottom of the milling jar. This situation causes the MA durations to be longer. Figure 1 shows the processing of mechanical alloying.

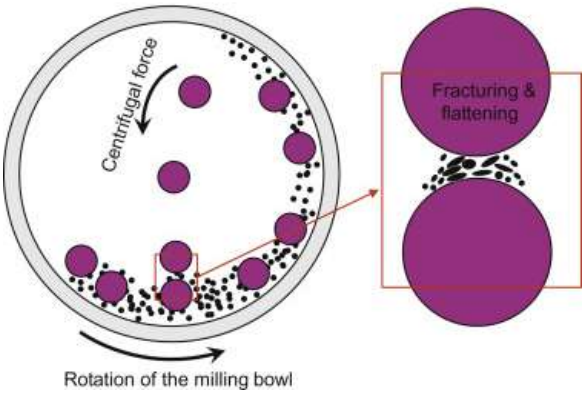

Figure 1. Mechanical alloying process [26, 27].

Different materials such as ceramic, stainless steel, chrome and sometimes rubber are used as milling balls. [28]. The mechanical alloying process has significant advantages, such as homogeneous distribution of the reinforcement in the matrix, the fine particle size of the powders, and thus increasing the strength of the material (increasing the dislocation density). Du et al. [29] distributed the graphene and SiC nanoparticles homogeneously to the particle boundaries of the AA7075 matrix. However, they noted that the SiC nanoparticles are between the graphene layers. Feijoo et al. [30] achieved good dispersion and integration of MWCNTs in AA7075 particles after 4 hours of grinding with high-energy ball milling. They found a reduction in grinding time by changing the rotational speed. Deaquino et al. [31] found that the particle size decreased by increasing the grinding time from 5 to 10 hours. It has been observed that the dust particles agglomerate exhibiting irregular shapes (similar to flakes) of different sizes. Salur et al. [32] stated that the ball milling time increase was influential in the uniform distribution of Y2O3 in the AA7075 matrix and the hardening of MMCs. However, prolonged grinding time (2–10 hours) was found to have a detrimental effect on tensile strength. Razavi et al. [33] stated that WC particles facilitate the grinding process, penetrate the aluminium powders, and show a good distribution. A change in particle size from micro to nano size was observed. Hernández et al. [34] observed that instability in the tetragonal structure occurred during the mechanical grinding of ZrO_2 powders. However, they state that the presence of ZrO_2 particles significantly affects the powder morphology and particle size of the matrix during the grinding process. A relatively good homogeneous distribution of ZrO_2 particles was observed after ball milling. Table 1 shows the parameters of the mechanical alloying of various AA7075 composites.

Table 1. Mechanical alloying parameters of various AA7075 composites.

Alloy	Reinforcement	Milling Time	Ball to Powder Ratio	Rotational Speed	Ref. Nu
AA7075	Graphene and SiC	6 h	5:1	50 rpm	[29]
AA7075	MWCNT	2 and 4 h	10:1	1300 and 1000 rpm	[30]
AA7075	Graphite	5 and 10 h	14:1	-	[31]
AA7075	Y_2O_3	0.25, 1, 1.5, 2, and 10 h	10:1	400 rpm	[32]
AA7075	TiO_2	10 min and 20 h	10:1	200 and 300 rpm	[35]
AA7075	WC	20 h	20:1	-	[33]
AA7075	Al_2O_3	12 h	10:1	250 rpm	[36]
AA7075	ZrO_2	2, 5, 10 and 15 h	8:1	120 rpm	[34]
AA7075	Graphene	30 min	10:1	240 rpm	[37]

When Table 1 is examined, it is seen that the mechanical alloying process is between 10 minutes and 20 hours. Furthermore, it is seen that the rotational speed is between 50 and 1300 rpm and the ball to powder ratio is between 5:1 and 20:1. In this study, the deformation of AA7075 powder was investigated with a three-dimensional ball mill designed and produced for use in mechanical alloying processes. In the experiments carried out, three different rotational speeds (150, 200 and 250 rpm), three different ball to powder ratios (5:1, 10:1 and 20:1) and three different durations (30, 60 and 90 min) were used.

In addition, the deformations occurring, the particle size analysis, and the per cent areas covered by the deformed powders were evaluated. Taguchi L9 orthogonal array was used for experimental design. Experimental results were analysed with analysis of variance, regression method, three-dimensional graphics, optical microscope and SEM images.

2. Materials and Methods

2.1. Three-dimensional ball mill

For this study, a new high-energy three-dimensional grinder was designed and produced, inspired by a commercially produced device [38], which has not been studied in the literature, to improve MA performance and reduce milling times. The milling performance will be increased with low heat generation and high homogeneity distribution, without agglomerations, with the three-dimensional rotational movement and the higher proportion of powder involved in the MA process compared to other devices and the continuous movement of the powders. The developed high-energy three-dimensional grinder was designed and produced to rotate the milling jar in three dimensions with the help of a single electric motor (1600 rpm, 50 hertz). As hardware, it has a structure that can provide rotation in both directions and the rotational speeds can be adjusted. The milling jar, driven by an electric motor, performs rotational movement and shaking movement in two axes. In two-dimensional (uniaxial) ball mills, the problem of powders sticking to the container walls and not mixing into the composition can be eliminated by adding another rotational movement (axis) perpendicular to the rotation axis and rotating it at a high rotational speed [39]. Therefore, in the milling system, the milling jar has been designed and produced in such a way that the rotation process in the X and Z axes, as well as the shaking movement in the Y-axis. In this way, it is ensured that the powders are included in the mixing and milling processes at a higher rate without sticking to the container wall. In Figure 2, the rotational and shaking axes of the three-dimensional ball mill are given.

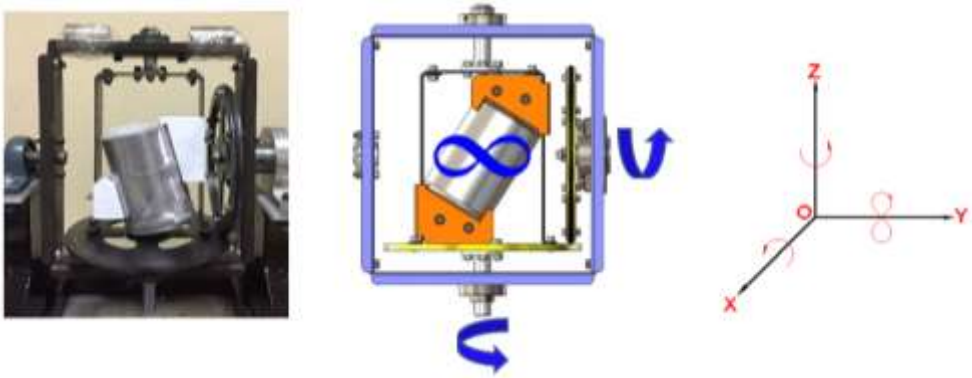

Figure 2. Three-dimensional ball mill and rotational-agitation axes.

2.2. Powder materials used in experiments and milling jar

AA7075 alloy powder with a spherical structure with an average size of <325 mesh was used for the experiments. The chemical, mechanical and physical properties of AA7075 alloy powder are shown in Tables 2 and 3.

Table 2. Chemical properties of AA7075 powder [42].

Al	Bal
Cu	1.57%
Fe	0.12%
Si	0.17%
Mn	≤0.01%
Mg	2.75%
Zn	5.46%
Ni	0.01%
Cr	0.24%

Table 3. Mechanical and physical properties of AA7075 powder [42].

Purity	99.5+ %
Average diameter	<325 mesh
Melting point	477-635 °C
Density	2.81 g/cm^3
Poisson's ratio	0.33
Tensile strength	572 MPa
Hardness	175 HV

Before the experiments, the image was taken with a SEM to examine the particle structure of the AA7075 alloy powder, and this image is shown in Figure 3. SEM analysis of the particles was performed by scanning electron microscopy (Gemini 500, Zeiss). After the images are analysed, the conclusion is that the AA7075 powder is mostly rounded in structure.

Figure 3. SEM image of AA7075 alloy powder (1000x).

Figure 4. Milling jar.

For the deformation experiments, 35 gr AA7075 alloy powder, 800 ml milling jar with rubber inner walls (Figure 4), and 10 mm diameter Zirconium Oxide (Zirconia) balls were used.

3 Experimental Design and Experiments

The Taguchi method also reduces the number of experiments [40]. The milling parameters and levels used in the experiments and selected as factors are given in Table 4.

Table 4. Factors and levels used in experiments.

Symbol	Factors	Levels		
		1	2	3
A	Rotational speed (rpm)	150	200	250
B	Ball to powder ratio	5:1	10:1	20:1
C	Milling time (min)	30	60	90

The L9 (3^3) orthogonal array was chosen for the experimental design. Therefore, nine experiments were performed using the Taguchi L9 orthogonal array instead of 27 for the full factorial experimental design. The particle size analysis of the particles was performed by particle size analyser (Malvern Mastersizer 2000) and optical micrographs of the deformed particles were performed by Celestron 44308 optical microscope. The experimental results obtained according to the factors and levels used in the deformation/milling experiments of the AA7075 alloy powder in the three-dimensional ball mill are given in Table 5.

Table 5. Particle size achieved in the experiments and per cent area of deformed particles.

	Factors			Results	
Test Number	A Rotational Speed (rpm)	B Ball to Powder Ratio	C Time (min)	Particle Size (D50, µm)	Deformation % Area
1	150	5:1	30	34	0.268
2	150	10:1	60	38	2.215
3	150	20:1	90	42	7.07
4	200	5:1	60	37	1.632
5	200	10:1	90	40	3.831
6	200	20:1	30	38	2.163
7	250	5:1	90	41	4.4
8	250	10:1	30	37	0.775
9	250	20:1	60	41	4.414

4. Evaluation of Experimental Results

4.1. Evaluation of experimental results with analysis of variance

The effects of the rotational speeds, the ball to powder ratio and the milling time on the deformation and particle size of the powders were analyzed by the ANOVA method. ANOVA values for the deformation of the powders and the achieved particle size are given in Table 6.

Table 6. ANOVA results for the particle size obtained in the experiments and the per cent areas covered by the deformed particles.

Variance Source	Degree of Freedom (DF)	Sum of Squares (SS)	Mean Square (MS)	F-Value	P-Value	Contribution (%)
Per cent area of deformation						
Rotational speed	1	0.0002	0.8344	10.09	0.086	0.00
Ball to powder ratio	1	8.9964	1.08654	13.14	0.068	24.44
Milling time	1	24.3815	0.05872	0.71	0.488	66.23
Error	2	0.1653	0.08267	-	-	0.45
Total	8	36.8115	-	-	-	-
Particle size (µm)						
Rotational speed	1	4.1667	0.31174	0.94	0.436	8.01
Ball to powder ratio	1	13.500	0.03061	0.09	0.790	25.96
Milling time	1	32.6667	0.66667	2.00	0.293	62.82
Error	2	0.6667	0.33333	-	-	1.28
Total	8	52.000	-	-	-	-

In Table 6, the per cent areas covered by the deformed particles were compared with ANOVA results according to the importance of the parameters, the milling time and ball to powder ratio in the chart effective. When the effects of the parameters are examined according to Table 6, the milling time is 66.23%, the ball to powder ratio is 24.44%, and the error is 0.45%. According to Table 6, the most influential factor affecting the deformation of particles is milling time, with a rate of 66.23%. After the milling time, the influential factor was the ball to powder ratio with 24.44%. When the effect of the parameters for the achieved particle size ANOVA results are analysed as a percentage, it is determined that the rotational speeds are 8.01%, the ball to powder ratio is 25.96%, the milling time is 62.82% and the error is 1.28%. According to Table 6, the most influential factor affecting the particle size is milling time, with a rate of 62.82%. After the milling time, the influential factor was determined as the ball to powder ratio with 25.96%.

4.2 Evaluation of experimental results with 3D graphics

Depending on the factors used in the experiments and their levels, the per cent deformation area in the particles obtained from the experimental study and the achieved particle size graphs are given in Figure 5. In Figure 5(a), the rotational speed of the three-dimensional ball mill and the effect of the ball to powder ratio on the deformation of the particles are shown as per cent area. In the graph, it is observed that the deformation of the particles increases as milling time increase. However, when the rotational speed and milling time are increased, the percentage areas of the deformed powders decrease. This situation caused the particles to break without deformation and thus to break into smaller pieces. However, the increase in rotational speed causes the balls to be affected by the centrifugal force. This situation restricts the movements of the balls. Although the balls are affected by the centrifugal force, the deformation of the powders increases due to the high collision speeds. Figure 5(a) shows that the maximum deformation is at 150 rpm rotational speed and 20:1 ball to powder ratio, while the minimum deformation is at 150 rpm rotational speed and 5:1 ball to powder ratio. In Figure 5(b), the effect of milling jar ball to powder ratio and milling time on the deformation of the particles is given as per cent area. The graph shows that the deformation of the particles increases as the ball to powder ratio and the milling time increase. As the ball to powder ratio increases, more balls in the milling jar affect the deformation, and the deformation of the particles increases with the increase of milling time. Figure 5(b) shows that the maximum deformation is at 20:1 ball to powder ratio and 90 min.

Figure 5(c) shows the effect of three-dimensional ball mill rotational speed and ball to powder ratio on particle size. When the graph is examined, it is observed that the particle size increases as the rotational speed and ball to powder ratio increase. When the rotational speed is increased to 250 rpm and 20:1 ball to powder ratio, although the balls are affected by the centrifugal force, the size of the particles increases due to the high collision speed of the balls. This situation caused the particles to break without deformation and thus to break into smaller pieces. The largest particle size reached in Figure 5(c) was obtained at 150 rpm rotational speed and 20:1 ball to powder ratio. The smallest particle size reached at 150 rpm rotational speed and 5:1 ball to powder ratio. The effect of the ball to powder ratio and milling time on particle size is given in Figure 5(d). In the graph, the particle size increases with the ball to

powder ratio and the milling time. With the increase in the number of balls included in the deformation process and the milling time, the high collision speed at high rotational speeds plays an influential role in increasing the particle size. The largest particle size reached in Figure 5(d) was obtained at 20:1 ball to powder ratio and 90 min. The smallest particle size reached at 5:1 ball to powder ratio and 30 min.

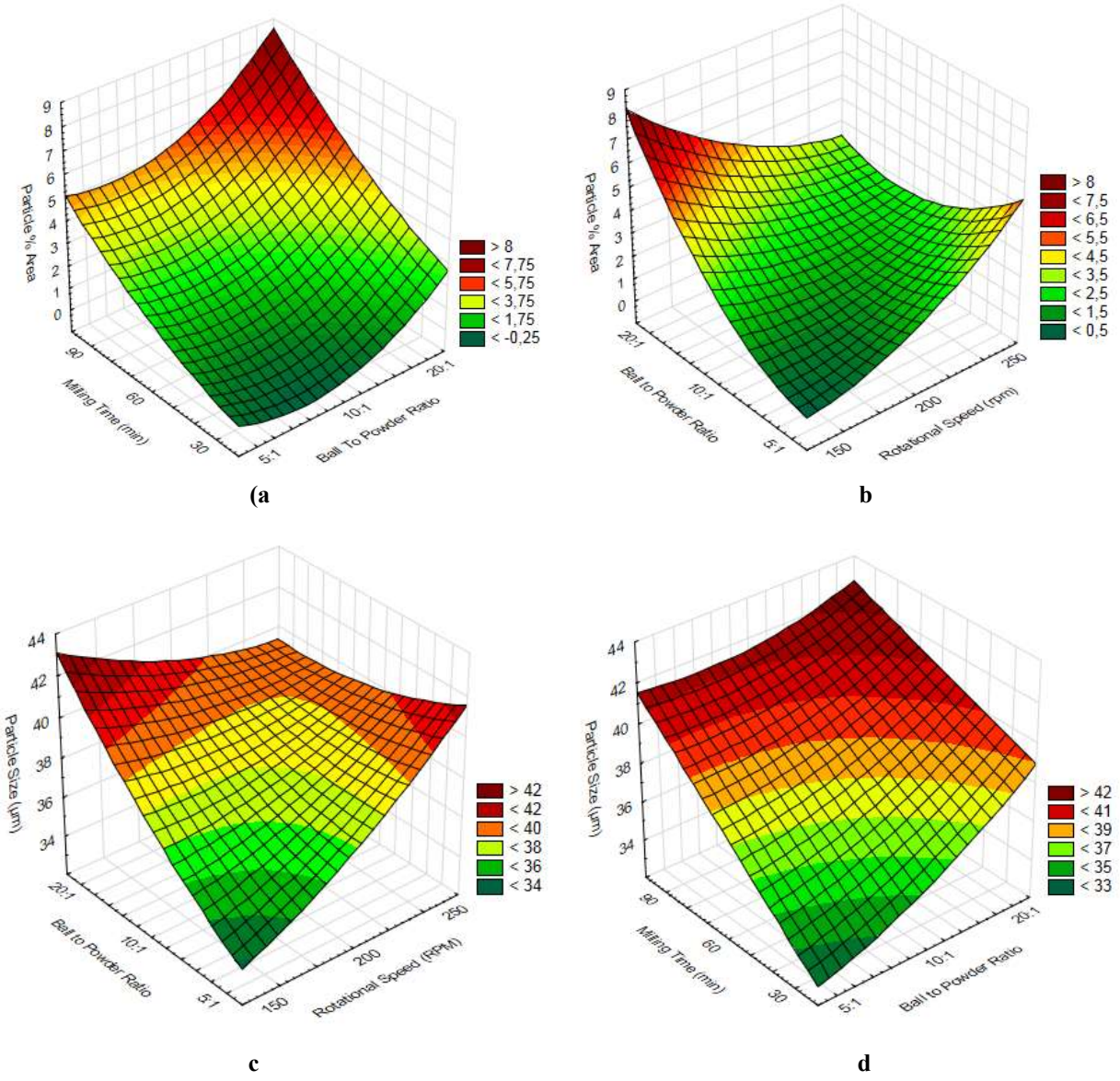

Figure 5. Effect of deformation in particles on per cent area and obtained particle size.

4.3. Regression method for experimental results

In the study, the level of relationship between the deformation of the particles and control factors was determined using the polynomial regression model. Multiple regression analysis is used to derive the estimation equations of the continuous dependent variables obtained through experimental designs with each combination of control factors [41]. The mathematical Equation 1 derived for the quadratic regression model is given to determine the deformation of the particles in per cent area.

$$\boldsymbol{Eq.1} = 11{,}02 - 0{,}1036 \times RPM - 2{,}979 \times BPR + 0{,}0231 \times T + 0{,}000259 \times RPM^2 + 1{,}051 \times BPR^2 + 0{,}000368 \times T^2 \quad \textbf{(1)}$$

Eq.1 expresses the predictive equation generated by using the control factors to calculate the deformation of the particles in per cent area. In Eq. 1, "RPM" is rotational speed, "BPR" is the ball to powder ratio, and "T" is time. Using Eq.1, the estimated deformation of the particles in per cent area for different parameters can be calculated.

The R^2 value for the per cent area occupied by the deformed AA7075 powders was 99.55%.

In order to determine the particle size to be reached, the mathematical equation derived for the quadratic regression model is given in Equation 2.

Eq. 2 expresses the predictive equation generated by the use of the control factors for calculating reached particle size. For the particle size equation to be reached for AA7075, the R^2 value was obtained as 98.72%.

$$\boldsymbol{Eq.2} = 37 - 0{,}0633 \times RPM - 0{,}50 \times BPR + 0{,}0778 \times T + 0{,}0002 \times RPM^2 + 0{,}5 \times BPR^2 \quad \textbf{(2)}$$

4.4 Evaluation of per cent area covered by deformed particles

The particles obtained from the experiments carried out at specific cycles, the ball to powder ratio, and milling times according to the test parameters and levels have adhered to a transparent tape measuring 10x10mm.

The images of the powders adhered to a transparent tape measuring 10x10mm were taken with an optical microscope at 20x magnification. The per cent areas covered by the deformed particles were determined with ImageJ, an image analysis program. Obtained images are given in Figure 6.

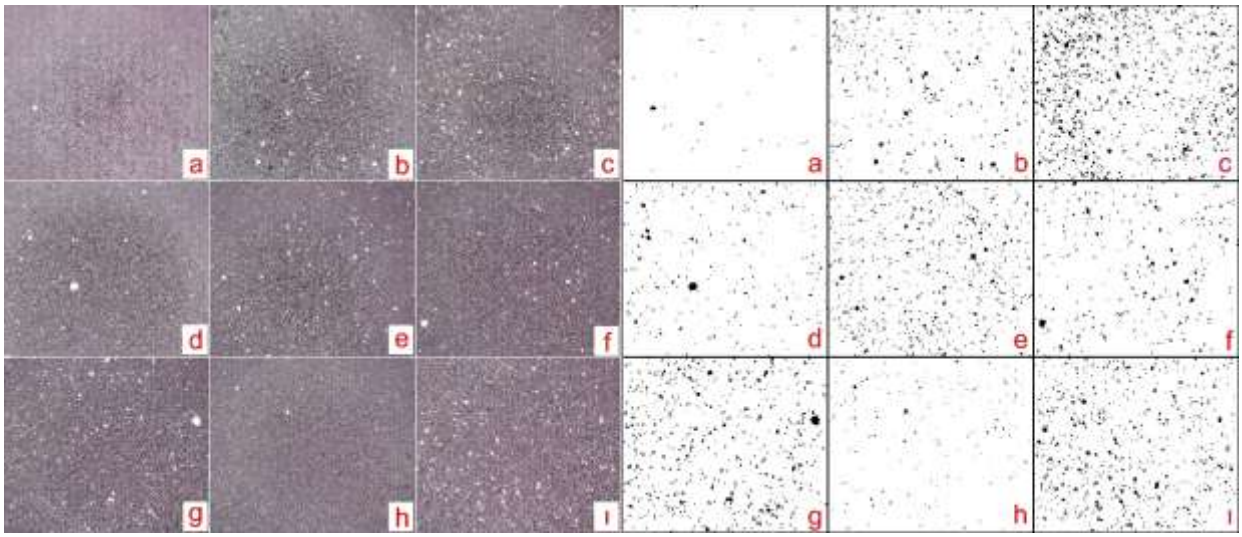

Figure 6. Optical microscope images of AA7075 alloy powder after milling: (a)150 rpm-5:1 ball to powder ratio-30 min, (b) 150 rpm-10:1 ball to powder ratio-60 min, (c) 150 rpm-20:1 ball to powder ratio-90 min, (d) 200 rpm-5:1 ball to powder ratio.

When Figure 6 is examined by the image analysis program in terms of the deformation of the particles, 0.268% in Figure 6(a), 2.215% in Figure 6(b), 7.07% in Figure 6(c), 1.632% in Figure 6(d), 3.831% in Figure 6(e), 3.831% in Figure 6(f), 2.163% in Figure 6(g), 0.775% in Figure 6(h), and 4.414% in Figure 6(i) was detected. When the test parameters are evaluated among themselves, it is observed that the particles' deformation is at least 150 rpm, 5:1 ball to powder ratio, 30 minutes (Figure 6(a)). It has been determined that the particles' deformation is a maximum at 150 rpm, 20:1 ball to powder ratio, 90 min (Figure 6). The most influential factor in the deformation of the particles stated in the results obtained by ANOVA analysis, from the most effective to the least effective, is the milling time, ball to powder ratio, and rotational speed. For this reason, the low milling time, ball to powder ratio, and milling time minimise the particles' deformation. Likewise, the increase in the milling time, ball to powder ratio, and milling time increase the particles' deformation ratios.

When the results obtained at the same rotational speeds are examined in terms of the ball to powder ratio and milling time, the percentage areas covered by the deforming particles increase significantly with the increase in the ball to powder ratio and milling time in all rotational speeds.

In particular, the high ball to powder ratio visibly increases the particles' deformation, even at low milling times. In the experiments, it is observed that the per cent deformation area obtained at 200 rpm-20:1 ratio-30 min is 1.33 times higher compared to 5:1 ball to powder ratio and 60 min at the same rotational speeds. Therefore, a more effective deformation process will be performed using the highest ball to powder ratio in a shorter milling time. With the mathematical model obtained to calculate the per cent deformation areas in particles by the regression method, the per cent deformation area calculated for 150 rpm-20:1 ratio-30 min is 10.63 and 1.29 times, respectively, higher than the other parameters in the same rotational speeds. As mentioned above, it has been proven that particles can be deformed more effectively in a shorter milling time at the highest ball to powder ratio.

In order to compare the milling performance of the designed and produced three-dimensional ball mill, the milling process was carried out at 150 rpm, 5:1, 10:1 and 20:1 ball to powder ratio and 30, 60, and 90 min. In addition, the images of the particles (350x) obtained from the experiments were taken by SEM to examine their performance in milling processes. It is given in Figure 7.

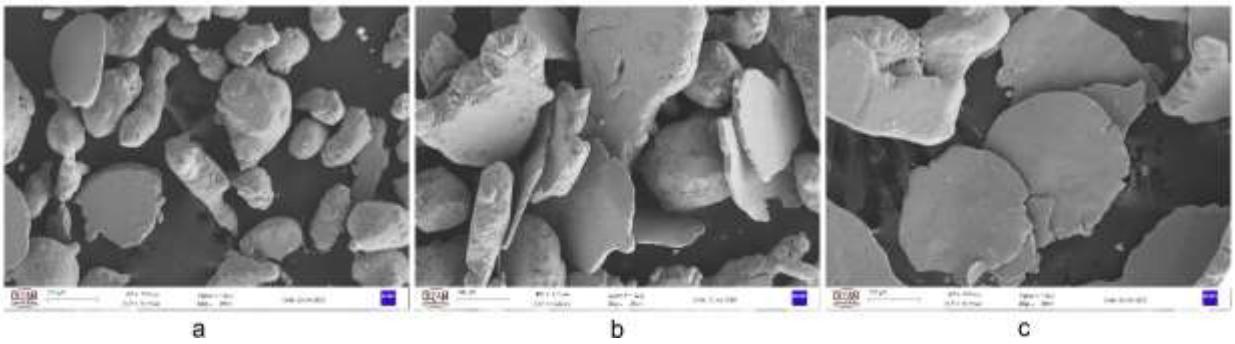

Figure 7. SEM images of ground AA7075 powders: 5:1 ball to powder ratio-30 min (a), 10:1 ball to powder ratio-60 min (b) and 20:1 ball to powder ratio-90 min (c).

When Figure 7 is examined, it is observed that the deformation of the particles increases with increasing milling times and ball to powder ratio by keeping the rotational speed constant. Thanks to the rotational and shaking movements obtained with the designed and manufactured device, the fact that the particles are in constant motion compared to other devices reveals a milling performance without the agglomeration with low heat generation.

5. Results and Discussion

In the study carried out, no studies were found in the literature with the three-dimensional ball mill. Therefore, in this study, the deformation of AA7075 powder, frequently used in the industry, was investigated using a three-dimensional ball mill developed, designed, and produced for use in mechanical alloying processes. Three different rotational speeds (150, 200 and 250 rpm), three different ball to powder ratios (5:1, 10:1 and 20:1) and three different milling times (30, 60 and 90 min) were used in the experiments. In addition, deformations occurring in the particles, particle size analysis, and per cent areas covered by the deformed particles were evaluated. The results obtained from the experimental study can be listed as follows;

- The best combination of the parameters used in the experiments was 150 rpm-20:1 ball to powder ratio-90 min.
- According to the results of the variance analysis applied for the per cent areas covered by the deforming particles, the most influential factor is the milling time, with a rate of 66.23%. On the other hand, the influential factor after the milling time is the ball to powder ratio with 24.44%.
- According to the variance analysis applied for the particle size obtained, the most influential factor is the milling time with a rate of 62.82%. After the milling time, the influential factor was the ball to powder ratio with 25.96%.
- According to the results of the analysis of variance, the rotational speed is not effective.
- In the three-dimensional graphics, it is observed that the deformation and particle size of the powders increase as the ball to powder ratio and milling time increase.
- By increasing the rotational speed to 250 rpm, the balls are affected by the centrifugal force. However, due to the high collision speed of the balls, there is an increase in the size and deformation of the particles.

- Thanks to the rotational and shaking movements obtained with the designed and manufactured device, it is observed that the powders are in constant motion compared to other devices and that it exhibits a milling performance without the agglomerations together with low heat generation.
- The fact that the walls of the milling jar used in the experiments are covered with rubber prevents the deformation mechanism that will occur between the balls and the milling jar wall. Therefore, using a zirconium oxide milling jar will increase the milling performance.
- The large diameters of the balls make the deformation of micron-sized particles difficult. However, deformation can be increased by choosing a smaller ball diameter.

6. Conclusion

AA7075 alloy powder, which is frequently used in the industry, was used for this study. The method used in the study can be used for the mechanical alloying of all aluminium alloys and metal matrix composites. However, designed and produced, the three-dimensional ball mill is thought to be more effective, especially in milling brittle materials.

Acknowledgement

Gazi University Scientific Research Projects supported this study with the project code 07/2019-26.

Author's Contributions

Gürkan SOY: Performed the experiments and results analysis.
Salih KORUCU: Prepared experimental method, supervised the experiment's progress, result in interpretation and helped in manuscript preparation.

Ethics

There are no ethical issues after the publication of this manuscript.

References

[1]. Panwar, N, Chauhan, A. 2018. Fabrication methods of particulate reinforced Aluminium metal matrix composite-A review. *Materials Today: Proceedings*; 5(2): 5933–5939.

[2]. Sharma, AK, Bhandari, R, Aherwar, A, Rimašauskiene, R, Pinca-Bretotean, C. 2020. A study of advancement in application opportunities of aluminum metal matrix composites. *Materials Today: Proceedings*; 26,: 2419–2424.

[3]. Imran, M, Khan, ARA. 2019. Characterization of Al-7075 metal matrix composites: A review. *Journal of Materials Research and Technology*; 8(3): 3347–3356.

[4]. Kaczmar, JW, Pietrzak, K, Wlosiński, W. 2000. Production and application of metal matrix composite materials. *Journal of Materials Processing Technology*; 106(1–3): 58–67.

[5]. Balokhonov, R, Romanova, V, Kulkov, A. 2020. Microstructure-based analysis of deformation and fracture in metal-matrix composite materials. *Engineering Failure Analysis*; 110: 104412.

[6]. Hao, XN, Zhang, HP, Zheng, RX, Zhang, YT, Ameyama, K, Ma, CL. 2014. Effect of mechanical alloying time and rotation speed on evolution of CNTs/Al-2024 composite powders. *Transactions of Nonferrous Metals Society of China (English Edition)*; 24(7): 2380–2386.

[7]. Pérez-Bustamante, R, Pérez-Bustamante, F, Estrada-Guel, I, Licea-Jiménez, L, Miki-Yoshida, M, Martínez-Sánchez, R. 1970. Effect of milling time and CNT concentration on hardness of CNT/Al2024 composites produced by mechanical alloying. *Materials Characterization*; 75: 13–19.

[8]. Karabulut, H, Türkmen, M. 2017. Effect of the amount of Si and aging durations in Al2024-Si alloyed composites produced by powder metallurgy method. *Omer Halisdemir University Journal of Engineering Sciences*; 6(1): 226–231.

[9]. Korucu, S, Soy, G. 2019. An Investigation on the Effects of Tungsten Carbide and Grafen Reinforcements to Mechanical Properties in the Aluminium Matrix Composites. *Düzce University Journal of Science and Technology*; 7(3): 1466–1487.

[10]. Taştan, M, Gökozan, H, Çavdar, PS, Soy, G, Çavdar, U. 2019. Analysis of artificial aging with induction and energy costs of 6082 Al and 7075 Al materials. *Revista de Metalurgia*; 55(1): 1–7.

[11]. Xia, H, Zhang, L, Zhu, Y, Li, N, Sun, Y, Zhang, J, Ma, H. 2020. Mechanical properties of graphene nanoplatelets reinforced 7075 aluminum alloy composite fabricated by spark plasma sintering. *International Journal of Minerals, Metallurgy and Materials*; 27(9): 1295–1300.

[12]. Pickens, JR. 1981. Aluminium powder metallurgy technology for high-strength applications. *Journal of Materials Science*; 16(6): 1437–1457.

[13]. Suryanarayana, C. 2001. Mechanical alloying and milling. *Progress in Materials Science*; 46(1–2): 1–184.

[14]. Soy, G, Korucu, S. 2022. Investigations On The Mechanical Alloying Properties Of Al 2024 Alloy By Three-Dimensional Ball Mill. *Surface Review and Letters*.

[15]. Ağaoğulları, D, Balcı, Ö, Öveçoğlu, ML. 2017. Effect of milling type on the microstructural and mechanical properties of W-Ni-ZrC-Y2O3 composites. *Ceramics International*; 43(9): 7106–7114.

[16]. Concas, A, Lai, N, Pisu, M, Cao, G. 2006. Modelling of comminution processes in Spex Mixer/Mill. *Chemical Engineering Science*; 61(11): 3746–3760.

[17]. Ebrahimi-Kahrizsangi, R, Abdellahi, M, Bahmanpour, M. 2015. Self-ignited synthesis of nanocomposite powders induced by Spex mills; modeling and optimizing. *Ceramics International*; 41(2): 3137–3151.

[18]. Alam, MA, Ya, HH, Azeem, M, Hussain, P Bin, Salit, MS bin, Khan, R, Arif, S, Ansari, AH. 2020. Modelling and optimisation of hardness behaviour of sintered Al/SiC composites using RSM and ANN: A comparative study. *Journal of Materials Research and Technology*; 9(6): 14036–14050.

[19]. Bor, A, Jargalsaikhan, B, Uranchimeg, K, Lee, J, Choi, H. 2021. Particle morphology control of metal powder with various experimental conditions using ball milling. *Powder Technology*; 394: 181–190.

[20]. Morsi, K, Esawi, A. 2007. Effect of mechanical alloying time and carbon nanotube (CNT) content on the evolution of aluminum (Al)-CNT composite powders. *Journal of Materials Science*; 42(13): 4954–4959.

[21]. Canakci, A, Varol, T, Erdemir, F. 2016. The Effect of Flake Powder Metallurgy on the Microstructure and Densification Behavior of B4C Nanoparticle-Reinforced Al–Cu–Mg Alloy Matrix Nanocomposites. *Arabian Journal for Science and Engineering*; 41(5): 1781–1796.

[22]. Almotairy, SM, Boostani, AF, Hassani, M, Wei, D, Jiang, ZY. 2020. Effect of hot isostatic pressing on the mechanical properties of aluminium metal matrix nanocomposites produced by dual speed ball milling. *Journal of Materials Research and Technology*; 9(2): 1151–1161.

[23]. Aksöz, S, Özdemir, AT, Bostan, B. 2013. Alloyed AA2014 aluminium powders synthesized with carbon and determined properties. *Journal of the Faculty of Engineering and Architecture of Gazi University*; 27(1): 109–115.

[24]. Gökmese, H, Bostan, B. 2014. Microstructural characterization and synthesis by mechanochemical method of nano particle Al2O3/B4C ceramic phase. *Journal of the Faculty of Engineering and Architecture of Gazi University*; 29(2): 289–297.

[25]. Şimşek, İ, Yıldırım, M, Tunçay, T, Özyürek, D, Şimşek, D. 2018. An investigation of Al-SiC composites produced by mechanical alloying/mechanical milling method. *Technological Applied Sciences*; 13(2): 165–171.

[26]. Yu, J, Yang, S, Kim, J, Lee, Y, Lim, KT, Kim, S, Ryu, SS, Jeong, H. 2020. A confidence interval-based process optimization method using second-order polynomial regression analysis. *Processes*; 8(10): 1206.

[27]. Costantino, U, Nocchetti, M, Gorrasi, G, Tammaro, L. Hydrotalcites in nanobiocomposites. In: Lagarón JM (ed) Multifunctional and nanoreinforced polymers for food packaging, Elsevier, 2011, pp 43–85.

[28]. Prakash, DS, Mariappan, R, Anand, JV, Sundar, DJ, Dinesh, K. 2018. A review on latest development of aluminium alloy metal matrix composite through powder metallurgy route. *International Journal of Mechanical and Production Engineering Research and Development*; 2018,: 235–241.

[29]. Du, XM, Zheng, KF, Zhao, T, Liu, FG. 2018. Fabrication and characterization of Al 7075 hybrid composite reinforced with graphene and SiC nanoparticles by powder metallurgy. *Digest Journal of Nanomaterials and Biostructures*; 13(4): 1133–1140.

[30]. Feijoo, I, Pena, G, Cristóbal, MJ, Cabeza, M, Rey, P. 2022. Effect of Carbon Nanotube Content and Mechanical Milling Conditions on the Manufacture of AA7075/MWCNT Composites. *Metals*; 12(6): 1020.

[31]. Deaquino-Lara, R, Gutiérrez-Castañeda, E, Estrada-Guel, I, Hinojosa-Ruiz, G, García-Sánchez, E, Herrera-Ramírez, JM, Pérez-Bustamante, R, Martínez-Sánchez, R. 2014. Structural characterization of aluminium alloy 7075-graphite composites fabricated by mechanical alloying and hot extrusion. *Materials and Design*; 53: 1104–1111.

[32]. Salur, E, Aslan, A, Kuntoğlu, M, Acarer, M. 2021. Effect of ball milling time on the structural characteristics and mechanical properties of nano-sized Y2O3 particle reinforced aluminum matrix composites produced by powder metallurgy route. *Advanced Powder Technology*; 32(10): 3826–3844.

[33]. Razavi, M, Mobasherpour, I. 2014. Production of aluminum nano-composite reinforced by tungsten carbide particles via mechanical milling and subsequent hot pressing. *International Journal of Materials Research*; 105(11): 1103–1110.

[34]. Hernández-Martínez, SE, Cruz-Rivera, JJ, Garay-Reyes, CG, Elias-Alfaro, CG, Martínez-Sánchez, R, Hernández-Rivera, JL. 2015. Application of ball milling in the synthesis of AA 7075-ZrO2 metal matrix nanocomposite. *Powder Technology*; 284: 40–46.

[35]. Karunanithi, R, Bera, S, Ghosh, KS. 2014. Electrochemical behaviour of TiO2 reinforced Al 7075 composite. *Materials Science and Engineering B: Solid-State Materials for Advanced Technology*; 190: 133–143.

[36]. Ruirui, W, Zheng, Y, Qiushu, L. 2017. Microstructure and mechanical properties of 7075 Al alloy based composites with Al2O3 nanoparticles. *International Journal of Cast Metals Research*; 30(6): 337–340.

[37]. Raj, RR, Yoganandh, J, Saravanan, MSS, Kumar, SS. 2021. Effect of graphene addition on the mechanical characteristics of AA7075 aluminium nanocomposites. *Carbon Letters*; 31(1): 125–136.

[38]. 3D Ball Mill (3D Reactor). http://www.nagaosystem.co.jp/serviceE.html/ (accessed at 17.09.2021).

[39]. Nagaosystem. https://www.nagaosystem.co.jp/ (accessed at 17.09.2021).

[40]. Samtaş, G, Korucu, S. 2019. Optimization of cutting parameters for surface roughness in milling of cryogenic treated EN AW 5754 (AlMg3) aluminum alloy. *Journal of Polytechnic*; 22(3): 665–673.

[41]. Samtaş, G, Korucu, S. 2019. The Optimization of Cutting Parameters Using Taguchi Method in Milling of Tempered Aluminum 5754 Alloy. *Düzce University Journal of Science and Technology*; 7: 45–60.

[42]. Aluminium 7075 Alloy Powder. https://nanografi.com/microparticles/aluminum-7075-alloy-powder-purity-99-5-size-325-mesh/ (accessed at 17.09.2021).